infrastructures

MDPI

Article

Effects of Differential Displacements Between the Ground Anchors in Suspension Bridges

Paolo Clemente

Formerly Italian National Agency for New Technologies, Energy and Sustainable Economic Development, ENEA Casaccia Research Centre, 00123 Rome, Italy; paolo.clemente59@gmail.com

Abstract: A simple model to evaluate the effects of relative displacements between the ground anchors of a suspension bridge is proposed. An equation system is defined, which allows for the evaluation of the structural response under a general displacement set of the ground anchor points. Then, the most interesting and likely cases are analyzed in detail with reference to a suspension bridge having geometrical and mechanical characteristics typical of a long-span bridge. A simple procedure for the assessment of variation in cable stress is also given, which can be used to choose the optimum values for stress in cables under dead loads, as a percentage of their strength. The results obtained showed that expected movements do not significantly impact the structure in its lifetime and that the effects become negligible for very long-span bridges. Finally, the results obtained can be easily used for the condition monitoring of suspension bridges.

Keywords: suspension bridges; long-span bridges; tectonic movements; relative displacements; cables

1. Introduction

The suspension bridge was probably one of the first types of bridge built by primitive men. They used ropes made of creeper plants between natural rocks. In the modern age, chains anchored to masonry towers, probably first in China and then in England and USA, and finally steel cables have been used. From the first half of the nineteenth century to the first half of the twentieth century, the span length of suspension bridges increased significantly, thanks to improvements in construction technologies, and also to the development of the elastic theory and then the deflection theory [1,2]. In 1931, the first bridge of more than 1000 m in span, the George Washington Bridge in New York, was completed [3]. In 1937, the Golden Gate Bridge was opened; it has a main span of 1240 m and is still a symbol of bridge engineering [4].

An increase in horizontal navigation clearances was necessary to accommodate the increasing size and volume of marine traffic. On the other hand, the lower cost of longer spans and shallow-water foundations is well known, compared to shorter spans with a greater number of deep-water foundations. Increases in the span also reduces the risk of ship collisions with piers.

Nowadays, the longest span in the world is that of the 1915 Canakkale Bridge at the Dardanelles, Turkey, completed in 2022. Its main span of 2023 m is just a little longer than the main span of the Akashi Kaikyo Bridge (1991 m) in Kobe, Japan, opened in 1998. Among the other long-span suspension bridges, it is worth remembering the Yangsigang Bridge in Wuhan, China (main span of 1700 m, opened in 2019), the Nansha Bridge in Dongguan, China (main span of 1688 m, opened in 2019), the Xihoumen Bridge between the islands of Jintang and Cezi, China (main span of 1650 m, opened in 2009), and the Great Belt Bridge between the Danish islands of Zealand and Funen (main span of 1624 m, opened in 1998). A suspension bridge with a main span of 3300 m has been designed to cross the Messina Strait, Italy, characterized by an innovative aerodynamic design [5,6], and finally, a three-span bridge, each of 5000 m, has been proposed for the Gibraltar Strait crossing [7].

Citation: Clemente, P. Effects of Differential Displacements Between the Ground Anchors in Suspension Bridges. *Infrastructures* **2024**, *9*, 211. https://doi.org/10.3390/infrastructures9110211

Academic Editor: Fabrizio Scozzese

Received: 17 October 2024
Revised: 8 November 2024
Accepted: 13 November 2024
Published: 20 November 2024

It is well known that the feasibility of longer suspension bridges is related to the implementation of new high-strength, light-weight materials but also to the availability of reliable monitoring systems that allow for continuous checking of structural conditions and activating alert systems, when necessary [8]. For this reason, in recent decades, significant applications for the structural health monitoring of bridges have been proposed [9–15]. On the other hand, recent resounding failures have brought to the forefront the issues of bridge safety and management in general [16–18].

A suspension bridge is usually designed to be used for a long time. This characteristic, in conjunction with the distance between its anchors to the ground, implies that it is very likely that a suspension bridge will be subject to tectonic shifts during its lifetime [19]. These are favoured and could be amplified in bridges crossing active faults. For example, tectonic shifts have been measured between the areas where the foundations of the pylons of the Messina Strait Bridge should be constructed, in Sicily and Calabria, respectively [20,21].

Relative displacements between the anchors of a suspension bridge to the ground can also occur during an earthquake, often with residual values at the end of the event, because of the very long distances between them and the obvious absence of rigid connections, even though suspension bridges are not very vulnerable to seismic actions, thanks to their very long vibration periods [22]. The effects could be traumatic when large shifts are caused by very strong earthquakes [23,24]. This happened to the Akashi Kaikyo Bridge in Kobe. The earthquake of 17 January 1995 caused a permanent displacement between the towers of about 1 m. At that moment, the bridge was under construction: only the two pylons had been erected and the main cables had been positioned [25]. The design was adapted, and the construction continued.

The effects of differential displacements between the ground anchors in suspension bridges have not been studied in depth in the past. On the contrary, an extensive bibliography exists on both experimental and numerical analyses of ordinary bridges crossing fault rupture zones [26,27]. For these, the variability of the seismic input between the different piers during an earthquake and the possibility of residual displacements have been particularly studied. Damage to bridges induced by surface fault rupture appeared during the 1906 San Francisco earthquake. Similar effects were also observed during more recent events [28]. Contemporarily, nonlinear models have been developed to analyze the behaviour of beam bridges crossing fault zones under earthquakes and to interpret the experimental data [29].

With reference to suspension bridges, anchors to the ground are subjected to different motions, especially in the case of near-fault earthquakes but also for different local seismic responses due to the subsoil characteristics. Jia et al. [30] carried out a detailed numerical analysis with a 3D model to evaluate the seismic performance of a long-span suspension bridge against fault-ground motions with different permanent displacements. The authors pointed out the necessity of a special seismic design to face bending moments at the bottom of the towers. Permanent displacements are responsible for large responses in suspension bridges, where stresses in main cables and vertical displacements of the deck are the main parameters to be controlled.

In this paper, a simple model is used to evaluate the effects related to tectonic shifts in suspension bridges and to follow the strains evolving over time based on the measurements of the displacements of the bridge-ground anchors. Only sensors located on the ground, where the towers and the cable-end anchors are, are strictly necessary, and satellite observations are sufficient to control their movements.

A general approach is first introduced, and then elementary cases are analyzed. This study refers mainly to long-span suspension bridges, for which the stiffening contribution of the girder to the structural behaviour becomes negligible, and the response is similar to that of the simple cables [31,32]. Therefore, the effects on the main cables and on the towers are evaluated without considering the contribution of the deck, which is supposed to be extremely flexible. Then, the effects on the deck are qualitatively analyzed as a consequence of the cable movements. The results are given in diagrams that can be used to

have threshold values for a preliminary check. Moreover, the same results can be managed to optimize the preliminary design of the bridge. A monitoring system is obviously needed to control the movements of the ground anchors and to plan any interventions in time.

2. Criteria and Procedures for a Simplified Assessment of Bridges

The following hypotheses are assumed, considering that this study refers to long-span suspension bridges:

- The main cables are anchored to the ground at their ends, A and D (Figure 1), but can slide at the tops of the towers, B and C.
- The deck is suspended from two parallel steel cables via hangers along the main span. Along the side spans, it may or may not be suspended from the main cables. In the following, the ends of the deck, M and Q, are supposed to be very close to the cable anchors A and D, respectively.
- The deck is vertically supported with anti-lifting systems at its ends, M and Q, where the longitudinal displacements (related to temperature, wind, and breaking actions) are allowed, while elastic constraints act in the transversal direction.
- At N and P, the deck is not constrained to the pylons in the vertical direction, while dampers limit the relative movements between the girder and the pylons, both in the longitudinal and transversal direction.
- Hangers are uniformly spaced along the three spans and, as usual, can be considered as infinitely rigid connections between the main cables and the deck, able to transfer axial actions only. A more detailed modelling should consider the geometrical nonlinearity.

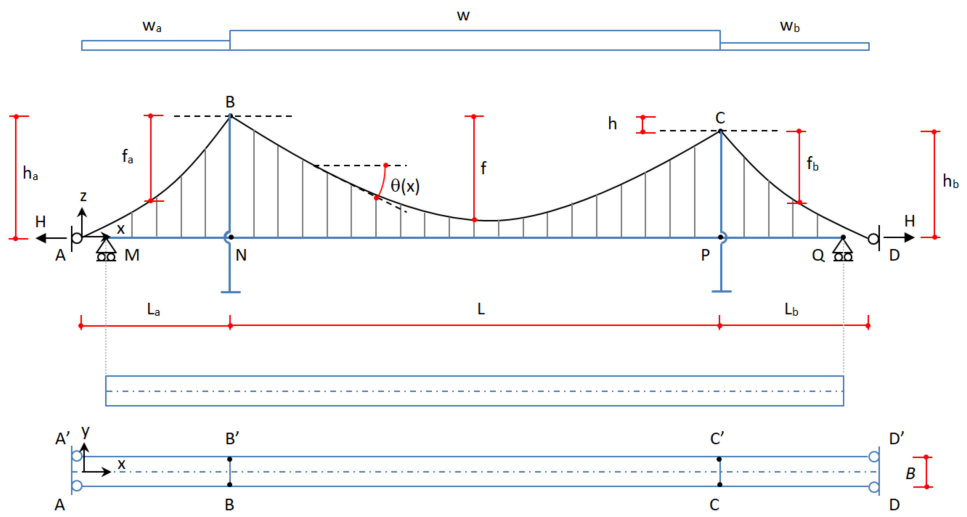

Figure 1. General model of a suspension bridge.

In the following passages, in order to maximize the effects on the deck, this will be supposed to be fully constrained in the transversal direction at M, N, P, and Q. Internal and external constraints are summarized in Table 1.

Table 1. Internal and external constraints.

Elements	Ext./Int.	Points	Constraint
Cables	External	A, D	$d_x = d_y = d_z = 0$
Cables–Towers	Internal	B, C	$\Delta d_y = \Delta d_z = 0$
Deck	External	M, Q	$d_y = d_z = 0$
Deck–Towers	Internal	N, P	$\Delta d_y = 0$

Each cable is subject to a uniform dead load w on the main span, which in long-span bridges is much higher than the travelling load. The side spans are subject to the dead

loads w_a and w_b, respectively. If the deck is suspended in the main span only, then loads w_a and w_b are just related to the self-weight of the cable. In long-span bridges, this is usually a high ratio of the total load. Instead, if the cable self-weight is negligible compared to the total dead load w, then the cable, subject to high axial forces at its ends, assumes an almost straight-line configuration.

3. Fundamental Equilibrium and Compatibility Equations of a Suspension Cable

The configuration of a single cable is identified by the coordinates of the joints A, B, C, and D (Figure 1). Suppose the cable is in a vertical plane in its natural configuration, then the geometrical characteristics can be derived from the coordinates of the joints.

Let us consider a generic cable on three spans, subject to uniformly distributed loads on each of them, and hanging from the points B and C (h being the difference in height between them). The equilibrium equations, which state the uniqueness of the horizontal component H of the forces in the cable, can be rewritten in the non-dimensional form (denoted by ˆ) for each of the three spans:

$$\hat{H} = \frac{H}{wL} = \frac{1}{8(f/L - h/2L)} = \frac{1}{8\left(\hat{f} - \hat{h}/2\right)} \tag{1a}$$

$$\hat{H} = \frac{w_i L_i}{wL} \cdot \frac{1}{8(f_i/L_i - h_i/2L_i)} = \hat{w}_i \hat{L}_i \cdot \frac{1}{8\left(\hat{f}_i - \hat{h}_i/2\right)} \quad (i = a,\ b) \tag{1b}$$

This is a system of three equations in the four unknowns $\hat{H}$, $\hat{f}$, $\hat{f}_a$, $\hat{f}_b$. Usually, we assume a value for $\hat{f}$ and deduce $\hat{H}$ from the first equation and then $\hat{f}_a$ and $\hat{f}_b$ from the second and third ones, respectively. These latest equations can be rewritten as follows:

$$\hat{f}_i = \frac{f_i}{L_i} = \frac{\hat{h}_i}{2} + \hat{w}_i \hat{L}_i \left(\hat{f} - \frac{\hat{h}}{2}\right) \qquad (i = a,\ b) \tag{2}$$

If we assume the cable shape to be parabolic, the deformed cable lengths in the three spans, under the loads w, w_a, and w_b, respectively, are given with good approximation by the following three relations:

$$\hat{\ell} = \frac{\ell}{L} = \left(1 + \frac{8}{3}\hat{f}^2 + \frac{\hat{h}^2}{2}\right) \tag{3a}$$

$$\hat{\ell}_i = \frac{\ell_i}{L} = \hat{L}_i \left(1 + \frac{8}{3}\hat{f}_i^2 + \frac{\hat{h}_i^2}{2}\right) \qquad (i = a,\ b) \tag{3b}$$

The hypotheses of uniformly distributed load and of parabolic shape are certainly convenient approximations but quite close to reality. In fact, the total permanent load is the sum of the deck weight, which is almost uniformly distributed, and the cable weight, which can be considered uniformly distributed, especially for low values of $\hat{f}$.

From H, we deduce the maximum axial force in the cable (at B or C) due to dead loads. From this force and the cross-sectional area A (defined on the basis of the maximum axial force under dead-plus-travelling loads) we deduce the maximum working stress $\sigma = \alpha f_d$ (f_d = design stress of the cables, $\alpha < 1$) under dead load w. Manipulating the relationship between A and σ, we can define the non-dimensional parameter:

$$\rho = \frac{wL}{8EA} = \frac{\alpha f_d}{E} \frac{1 - \hat{h}/2\hat{f}}{\sqrt{1/\hat{f}^2 + 16}} \tag{4}$$

which is a function of the mechanical (i.e., the tension $\sigma = \alpha f_d$ and Young's modulus E) and geometrical (i.e., the sag ratio $\hat{f}$ and the height $\hat{h}$) configuration of the cable under dead

loads w. If $\hat{h} = 0$, Equation (4) simplifies as $\rho = \alpha f_d / E\sqrt{1/\hat{f}^2 + 16}$. The initial undeformed lengths of the three portions of the cable in the three spans are given by the following approximate relations, given in non-dimensional form:

$$\hat{\ell}_0 = \frac{\ell_0}{L} = \left[\left(1 + \frac{8}{3}\hat{f}^2 + \frac{\hat{h}^2}{2}\right) - \frac{\rho}{\left(\hat{f} - \hat{h}/2\right)}\left(1 + \frac{16}{3}\hat{f}^2 + \hat{h}^2\right)\right] \tag{5a}$$

$$\hat{\ell}_{i0} = \frac{\ell_{i0}}{L} = \hat{L}_i\left[\left(1 + \frac{8}{3}\hat{f}_i^2 + \frac{\hat{h}_i^2}{2}\right) - \frac{\rho}{\left(\hat{f} - \hat{h}/2\right)}\left(1 + \frac{16}{3}\hat{f}_i^2 + \hat{h}_i^2\right)\right] \quad (i = a,\ b) \tag{5b}$$

In all the above equations, the contributions to the cable length variation due to shape change and the axial force are apparent. The total length of the undeformed cable is given by the following sum:

$$\hat{\ell}_{t0} = \hat{\ell}_{a0} + \hat{\ell}_0 + \hat{\ell}_{b0} \tag{6}$$

4. Effects of Relative Displacements Between the Ground Anchors: General Approach

The displacements of joints A, B, C, and D are independent of each other. If these joints are subject to a displacement system, the geometrical characteristics of the cable change as well as the axial force in it.

Consider a suspension bridge with two parallel main cables at the sides of the deck, as usual. Suppose that the anchors to the ground are subject to a displacement system for which the cables keep being parallel (their distance in y direction does not change) and the abscissas of the corresponding anchors are always equal (A_1 and A'_1, etc.); i.e., they behave as a unique cable (Figure 2). The case of a rotation of a pylon will be considered separately later.

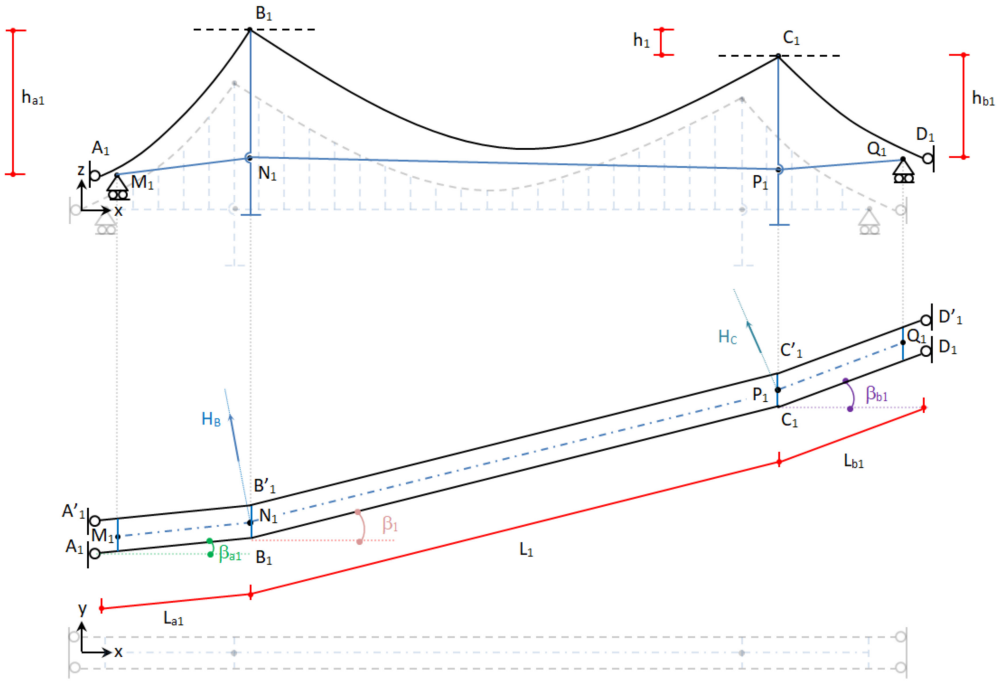

Figure 2. New configuration: longitudinal view and plan view.

In Figure 2, the longitudinal view of a new geometrical configuration of the cable and the deck is shown, supposing that all displacements occur in the positive directions of the axes. Moreover, the end points of the deck, M and Q, are subject to the same displacement of A and D, respectively, which is reasonable if the distances between them are very short, as supposed.

Denoting the new geometrical coordinates by the subscript "1", the new span lengths of each cable change as in Figure 2.

As already said, the entire cable is supposed to be on a single vertical plane in its natural configuration, but it could be not when a displacement system has occurred. In fact, each span may develop on a different vertical plane. The angles between each new vertical plane and the previous one are given by (positive if counter-clockwise, Figure 3):

$$\beta_1 = \arctan\left(\frac{y_{C1} - y_{B1}}{x_{C1} - x_{B1}}\right) \tag{7a}$$

$$\beta_{a1} = \arctan\left(\frac{y_{B1} - y_{A1}}{x_{B1} - x_{A1}}\right) \tag{7b}$$

$$\beta_{b1} = \arctan\left(\frac{y_{D1} - y_{C1}}{x_{D1} - x_{C1}}\right) \tag{7c}$$

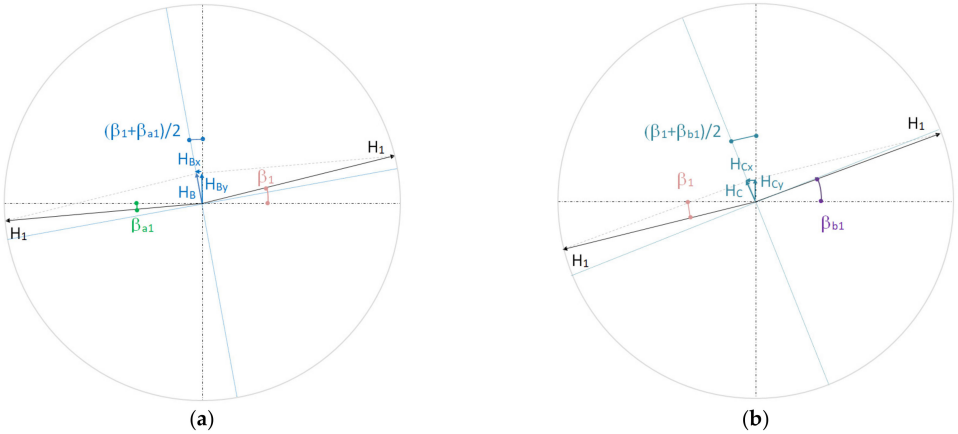

(**a**) (**b**)

Figure 3. Details of angles between the new planes at (**a**) pylon B and (**b**) pylon C.

For the hypothesis establish, the pylons are still parallel to the y direction ($x_{B1} = x_{B/1}$, $x_{C1} = x_{C/1}$). For the equilibrium in the horizontal plane, the horizontal forces in the new configuration can be written as

$$\hat{H}_1 = \frac{H_1}{wL} = \frac{L_1}{L} \cdot \frac{1}{8(f_1/L_1 - h_1/2L_1)} = \frac{\hat{L}_1}{8\left(\hat{f}_1 - \hat{h}_1/2\right)} \tag{8a}$$

$$\hat{H}_1 = \frac{w_i L_{i1}}{wL} \cdot \frac{1}{8(f_{i1}/L_{i1} - h_{i1}/2L_{i1})} = \frac{\hat{w}_i \hat{L}_{i1}}{8\left(\hat{f}_{i1} - \hat{h}_{i1}/2\right)} \quad (i = a,\ b) \tag{8b}$$

When $\hat{f}_1$ has been fixed, $\hat{H}_1$, $\hat{f}_{a1}$, and $\hat{f}_{b1}$ can be found from the first equilibrium equation and from the second and third ones, which can be rewritten as

$$\hat{f}_{i1} = \frac{f_{i1}}{L_{i1}} = \frac{\hat{h}_{i1}}{2} + \hat{w}_i \hat{L}_{i1}\left(\hat{f}_1 - \frac{\hat{h}_1}{2}\right) \qquad (i = a,\ b) \tag{9}$$

The solution can be found with an iteration procedure, which can be started by assigning a first tentative value of $\hat{f}_1$, calculating the corresponding new values of $\hat{H}_1$, $\hat{f}_{a1}$, and $\hat{f}_{b1}$, and verifying that the total length of the cable remains constant. The initial undeformed lengths of the three portions of the cable in the new three spans are

$$\hat{\ell}_{10} = \frac{\ell_1}{L} = \hat{L}_1\left[\left(1 + \frac{8}{3}\hat{f}_1^2 + \frac{\hat{h}_1^2}{2}\right) - \frac{\rho}{\hat{f}_1 - \hat{h}_1/2}\hat{L}_1\left(1 + \frac{16}{3}\hat{f}_1^2 + \hat{h}_1^2\right)\right] \tag{10a}$$

$$\hat{\ell}_{i10} = \frac{\ell_{i1}}{L} = \hat{L}_{i1}\left[\left(1 + \frac{8}{3}\hat{f}_{i1}^2 + \frac{\hat{h}_{i1}^2}{2}\right) - \hat{w}_i\hat{L}_{i1}\frac{\rho}{\hat{f}_{i1} - \hat{h}_{i1}/2}\left(1 + \frac{16}{3}\hat{f}_{i1}^2 + \hat{h}_{i1}^2\right)\right] \ (i = a,\ b) \tag{10b}$$

respectively, and the compatibility condition can be written as follows:

$$\hat{\ell}_{a10} + \hat{\ell}_{10} + \hat{\ell}_{b10} = \hat{\ell}_{a0} + \hat{\ell}_0 + \hat{\ell}_{b0} \tag{11}$$

The horizontal forces H_1 determine horizontal actions on the towers (Figure 3), with both transversal and longitudinal components (according to the global reference system). In the following passages, these are calculated in a linear analysis, i.e., neglecting the deflections of the towers.

The forces acting at the top of the pylons in the transversal global direction y are

$$\hat{H}_{By} = \frac{H_{By}}{H_1} = (\sin\beta_1 - \sin\beta_{a1}) \tag{12a}$$

$$\hat{H}_{Cy} = \frac{H_{Cy}}{H_1} = (\sin\beta_{b1} - \sin\beta_1) \tag{12b}$$

while those in the longitudinal global direction x are

$$\hat{H}_{Bx} = \frac{H_{Bx}}{H_1} = (\cos\beta_1 - \cos\beta_{a1}) \tag{13a}$$

$$\hat{H}_{Cx} = \frac{H_{Cx}}{H_1} = (\cos\beta_{b1} - \cos\beta_1) \tag{13b}$$

5. Elementary Cases

The previous relationships, deduced for the general case, can be simplified in practice. In fact, it is usually (Figure 4)

$$h_a = h_b\ , h = 0\ , L_a = L_b \tag{14a}$$

$$x_A = x_{A'}\ , x_B = x_{B'}\ , x_C = x_{C'}\ , x_D = x_{D'} \tag{14b}$$

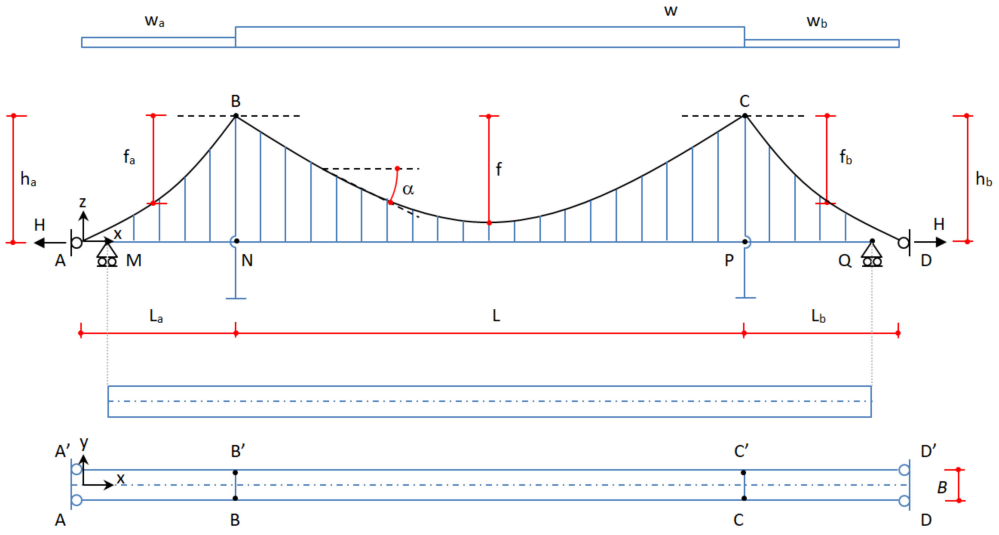

Figure 4. Investigated suspension bridge model.

In the following numerical investigation, the geometrical values $\hat{f} = 1/11$, $\hat{L}_a = \hat{L}_b = 0.33$, and $\hat{h}_a = \hat{h}_b = 0.3$ have been assumed. The material is characterized by $\alpha f_d/E = 0.005$, with α approximately equal to 0.90. With these geometrical and mechanical values, it is $\rho = 0.427 \cdot 10^{-3}$. The geometrical and mechanical characteristics considered are typical of very long-span bridges.

For the load ratios $\hat{w}_a = w_a/w$ and $\hat{w}_b = w_b/w$, the following two limit values have been considered:

- $\hat{w}_a = \hat{w}_b = 1$, for bridges in which all the three spans are suspended from the cables.
- $\hat{w}_a = \hat{w}_b = 0.5$, for bridges having only the main span suspended from the cables. In the case of short-span bridges with side spans not suspended from the main cables, it is often assumed that $\hat{w}_a = \hat{w}_b \approx 0$. However, this limit case is out of the scope of this paper.

Some basic cases of relative displacements between the anchors to the ground of a suspension bridge are studied herein. These are the longitudinal, vertical, and transversal relative displacements and the rotation of one tower around its vertical axis. In order to include all possible cases, the ranges of variability of the displacements considered are deliberately much larger than the realistic ones. For each case, the effects on the cables in terms of sag ratio and horizontal force are first analyzed, supposing that the deck has no bending stiffness both in the vertical and transversal plane, so that it just follows the movements of the cables in all spans. Then, the effects on the deck, connected to the cables by means of the hangers, are also analyzed, although only qualitatively. It is worth noting that more sophisticated models should account for the nonlinearity connected to the transversal interaction of cables and deck, which behave like a pendulum. With reference to the hangers, recent studies demonstrated that single-suspender loss can significantly affect only structural members in the immediate vicinity, while the rest of the bridge is not affected [33].

5.1. Longitudinal Relative Displacements

The previously discussed relationships are greatly simplified if only longitudinal displacements are acting on the structure. Two elementary cases are considered in the following passages. In the first one, the shift is due to a distortion in the right-side span, and in the second case, the distortion is supposed to occur in the main span.

5.1.1. Anchor D Subject to a Longitudinal Displacement

In this case, $d_{Dx} \neq 0$, while $d_{Ax} = d_{Bx} = d_{Cx} = 0$, and only the right-side span changes (Figure 5):

$$L_{b1} = L_b + d_{Dx} \tag{15}$$

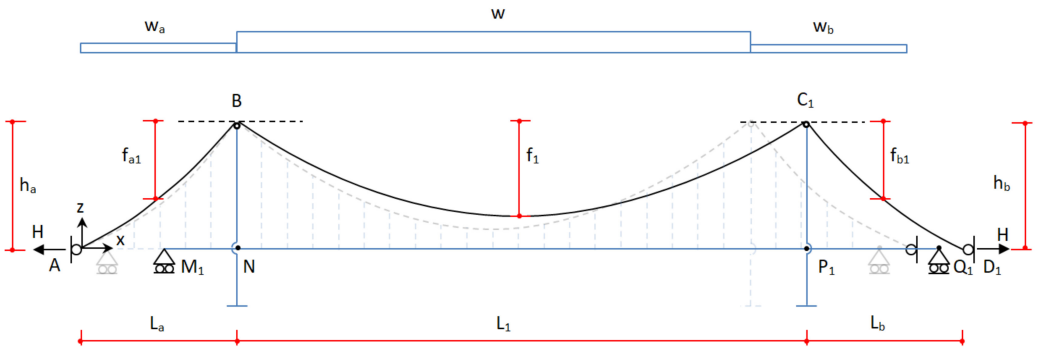

Figure 5. Effects due to $\hat{d}_{Dx} \neq 0$.

In Figure 6a, the diagrams of $\hat{f}_1$ versus displacement $\hat{d}_{Dx}$ are plotted for the two limit values of the load ratios $\hat{w}_a = \hat{w}_b$, while the variation in the horizontal force $\hat{H}_1$ is shown in Figure 6b. The behaviour is almost linear for low displacements and becomes nonlinear only for high values of $\hat{d}_{Dx}$. A certain variation in the sag ratio and the horizontal force can be observed even for low value of $\hat{d}_{Dx}$.

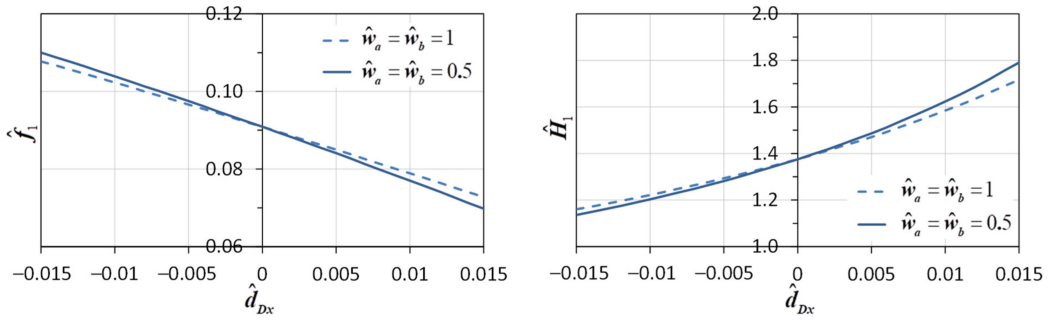

Figure 6. Variation in (**a**) $\hat{f}_1$ and (**b**) $\hat{H}_1$ due to $\hat{d}_{Dx} \neq 0$.

With reference to the deck, it is expected that the hangers will no longer be vertical but inclined, determining a global longitudinal movement of the deck, which should be absorbed by the bearings at Q and at M. Moreover, the deck will be subject to traction, and the shortest hangers, especially those along the right-side span, could suffer a significant stress increment.

5.1.2. Both C and D Subject to the Same Longitudinal Displacement

In this case, $d_{Cx} = d_{Dx} \neq 0$, while $d_{Ax} = d_{Bx} = 0$, and only the main span length changes (Figure 7):

$$L_1 = L + d_{Cx} \tag{16}$$

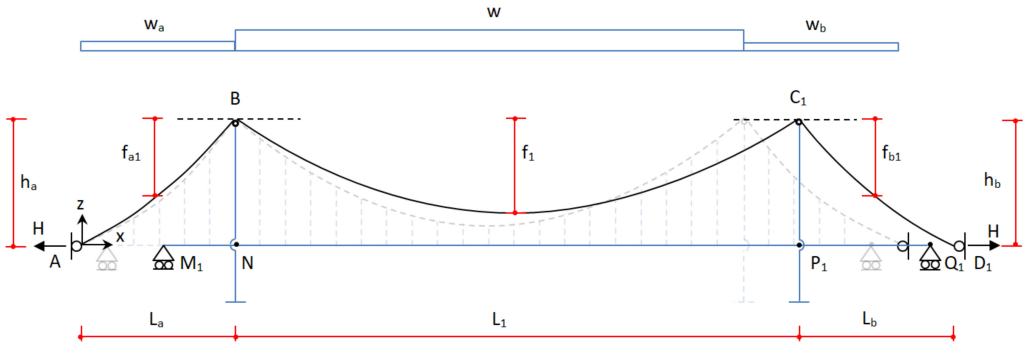

Figure 7. Effects of $\hat{d}_{Cx} = \hat{d}_{Dx} \neq 0$.

Figure 8 show the diagrams of the sag ratio $\hat{f}_1$ and the horizontal force $\hat{H}_1$ versus the longitudinal displacement $\hat{d}_{Cx} = \hat{d}_{Dx}$. The nonlinear behaviour is apparent for high values of the displacement. It is worth noting that, for a fixed value of the shift, this case ($\hat{d}_{Cx} = \hat{d}_{Dx} \neq 0$) causes effects a little greater than the previous one (only $\hat{d}_{Dx} \neq 0$).

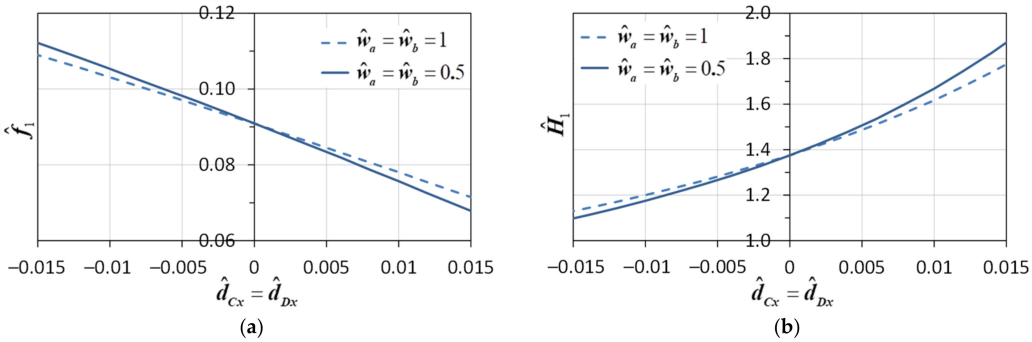

Figure 8. Variation in (**a**) $\hat{f}_1$ and (**b**) $\hat{H}_1$ due to $\hat{d}_{Cx} = \hat{d}_{Dx} \neq 0$.

Regarding the deck and the hangers, the effects qualitatively assessed are similar to those described in the previous case.

5.2. Vertical Relative Displacements

Two elementary cases of vertical shifts are considered in the following passages. In the first one, the shift is due to a vertical displacement of anchor D; in the second case, the distortion is supposed to occur in the main span, which translates into a vertical displacement of both joints C and D.

5.2.1. Anchor D Subject to a Vertical Displacement

In this case, $d_{Dz} \neq 0$, while $d_{Az} = d_{Bz} = d_{Cz} = 0$ (Figure 9). All the geometrical characteristics of the cable remain constant, except for the right-side height:

$$h_{b1} = h_b - d_{Dz} \tag{17}$$

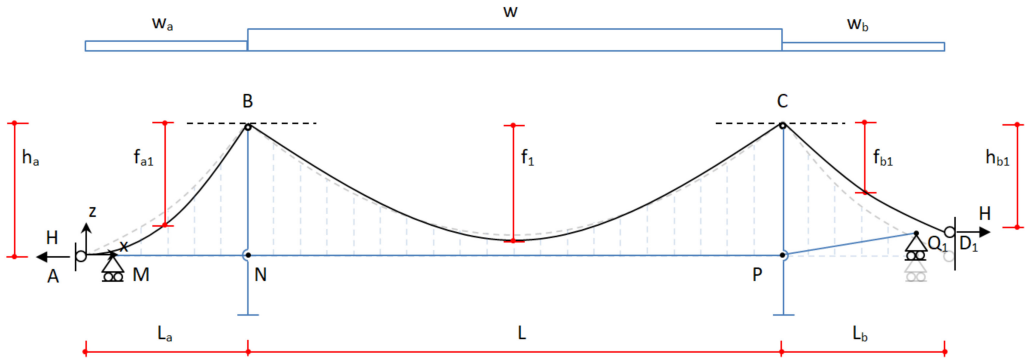

Figure 9. Effects of $\hat{d}_{Dz} \neq 0$.

Even if the lengths of the spans remain constant, the sag ratios of each span change. In Figure 10a, the diagrams of $\hat{f}_1$ versus the displacement $\hat{d}_{Dz}$ are plotted for the two limit values of the load ratios $\hat{w}_a = \hat{w}_b$, while Figure 10b shows the variation in the horizontal force $\hat{H}_1$. They both vary almost linearly for low values of the vertical displacement.

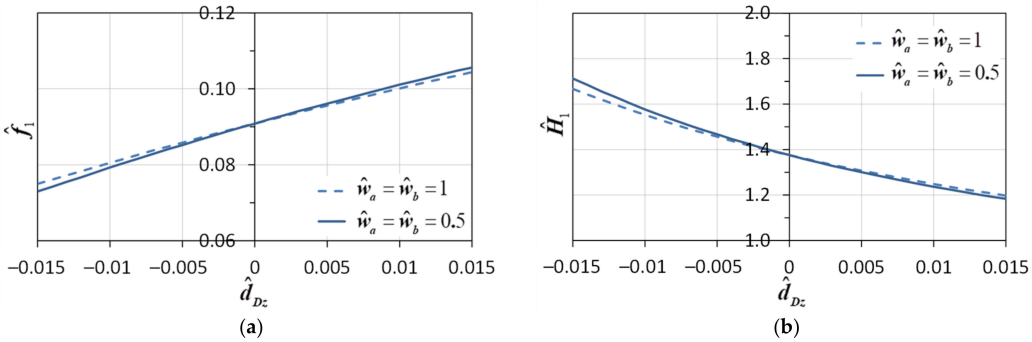

Figure 10. Variation in (**a**) $\hat{f}_1$ and (**b**) $\hat{H}_1$ due to $\hat{d}_{Dz} \neq 0$.

In terms of global behaviour, if Q is subject to the same vertical displacement as D, then the right-side span follows the main cables with limited stresses.

5.2.2. Both C and D Subject to the Same Vertical Displacement

In this case, $d_{Cz} = d_{Dz} \neq 0$, while $d_{Az} = d_{Bz} = 0$. All the geometrical characteristics of the cable remain constant, except for the difference in height between the two towers (Figure 11):

$$h_1 = h + d_{Cz} \tag{18}$$

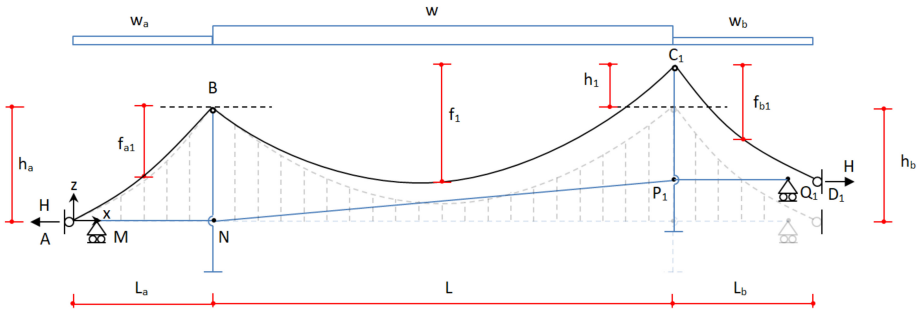

Figure 11. Effects of $\hat{d}_{Cz} = \hat{d}_{Dz} \neq 0$.

Figure 12a,b show the diagrams of the sag ratio $\hat{f}_1$ and the horizontal force $\hat{H}_1$ versus the vertical displacement $\hat{d}_{Cx}$ (=$\hat{d}_{Dx}$), respectively. In this case, the diagrams are obviously symmetric with reference to the starting point ($\hat{d}_{Cz} = \hat{d}_{Dz}$ =0). An uplift of D alone has greater effects than a simultaneous uplift of joints C and D of equal magnitude.

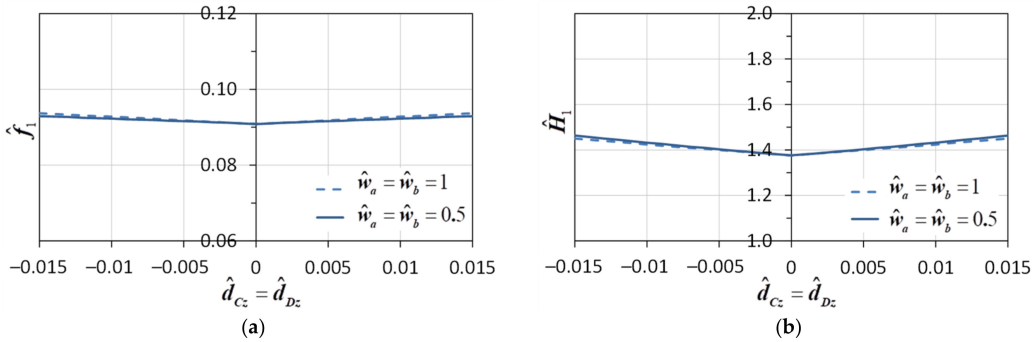

Figure 12. Variation in (**a**) $\hat{f}_1$ and (**b**) $\hat{H}_1$ due to $\hat{d}_{Cz} = \hat{d}_{Dz} \neq 0$.

With the same hypothesis as that of the previous case, it is expected that the deck is pulled up by the main cables, especially in the main and right-side spans, and the stresses are generally low.

5.3. Transversal Relative Displacements

Two cases are also considered for transversal shifts, the first relative to a displacement of D along y, and the second relative to a displacement of both C and D in y direction.

5.3.1. Anchor D Subject to a Transversal Displacement

In this case, $d_{Dy} \neq 0$, while $d_{Ay} = d_{By} = d_{Cy} = 0$ (Figure 13). Then, the length L_b and the angle β_b change as follows:

$$L_{b1} = \sqrt{L_b^2 + d_{Dy}^2} \qquad \beta_{b1} = \arctan\left(d_{Dy}/L_b\right) \tag{19}$$

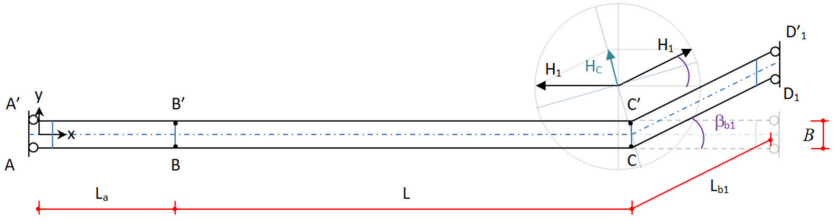

Figure 13. Effects of $d_{Dy} \neq 0$.

The span length variations are negligible and so are the sag ratio variations (Figure 14a). In Figure 14b, the diagrams of the horizontal force $\hat{H}_1$ versus the displacement $\hat{d}_{Dy}$ are plotted for the two limit values of the load ratios $\hat{w}_a = \hat{w}_b$. Figure 14c,d show the values

of the transversal force $\hat{H}_{Cy} = H_{Cy}/wL$ and the longitudinal force $\hat{H}_{Cx} = H_{Cx}/wL$ on the pylon at C. As one can see, the values are very low but could be important for long-span bridges, especially the transversal force.

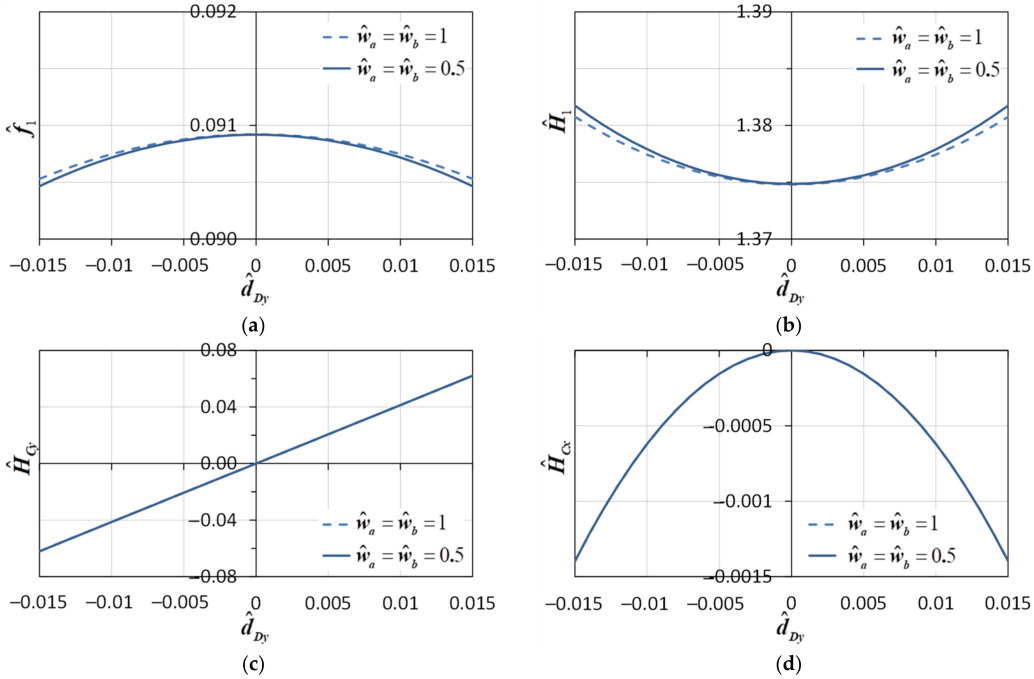

Figure 14. Variation in (**a**) $\hat{f}_1$, (**b**) $\hat{H}_1$, (**c**) $\hat{H}_{Cy}$ and (**d**) $\hat{H}_{Cx}$ due to $\hat{d}_{Dy} \neq 0$.

The transversal displacement of D and D', which is followed by the same displacement of Q, could determine the increased stresses in the deck. If the four transversal constraints at M, N, P, and Q are supposed to be rigid, then the transversal bending moments at N and P will be approximatively equal to $-3EI_z/L \cdot \hat{d}_{Dy}$ and $8EI_z/L \cdot \hat{d}_{Dy}$, respectively. The transversal forces on the pylons will be $-20EI_z/L^2 \cdot \hat{d}_{Dy}$ and $35EI_z/L^2 \cdot \hat{d}_{Dy}$ at B and C, respectively. If the constraints are elastic or viscous-elastic, as usual to mitigate the effects of horizontal and seismic actions, the values of bending moments and transversal forces will be lower that those given above.

5.3.2. Both C and D Subject to the Same Transversal Displacement

In this case, $d_{Cy} = d_{Dy} \neq 0$, while $d_{Ay} = d_{By} = 0$ (Figure 15), and the main span and the angle β_1 change as follows:

$$L_1 = \sqrt{L^2 + d_{Cy}^2} \qquad \beta_1 = \arctan\left(d_{Cy}/L\right) \tag{20}$$

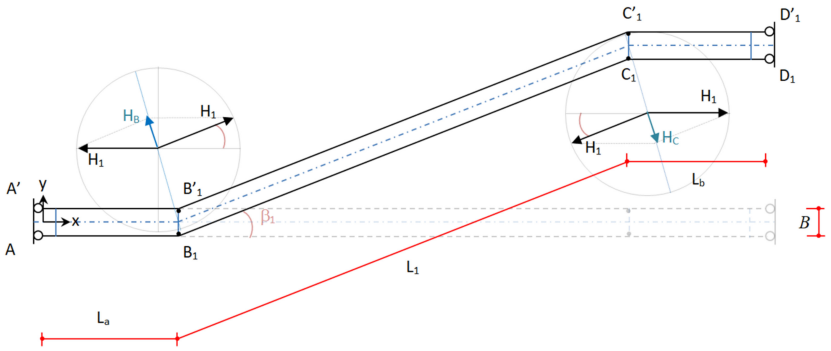

Figure 15. Effects of $d_{Cy} = d_{Dy} \neq 0$.

Span and sag ratio variations are very low (Figure 16a). In Figure 16b, the diagrams of the horizontal force $\hat{H}_1$ versus the displacement $\hat{d}_{Cy} = \hat{d}_{Dy} \neq 0$ are plotted for the two limit values of the load ratios $\hat{w}_a = \hat{w}_b$. Figure 16c,d show the values of the transversal force $\hat{H}_{Cy} = H_{Cy}/wL$ and the longitudinal force $\hat{H}_{Cx} = H_{Cx}/wL$ on the pylon. As in the previous case, the values are quite low.

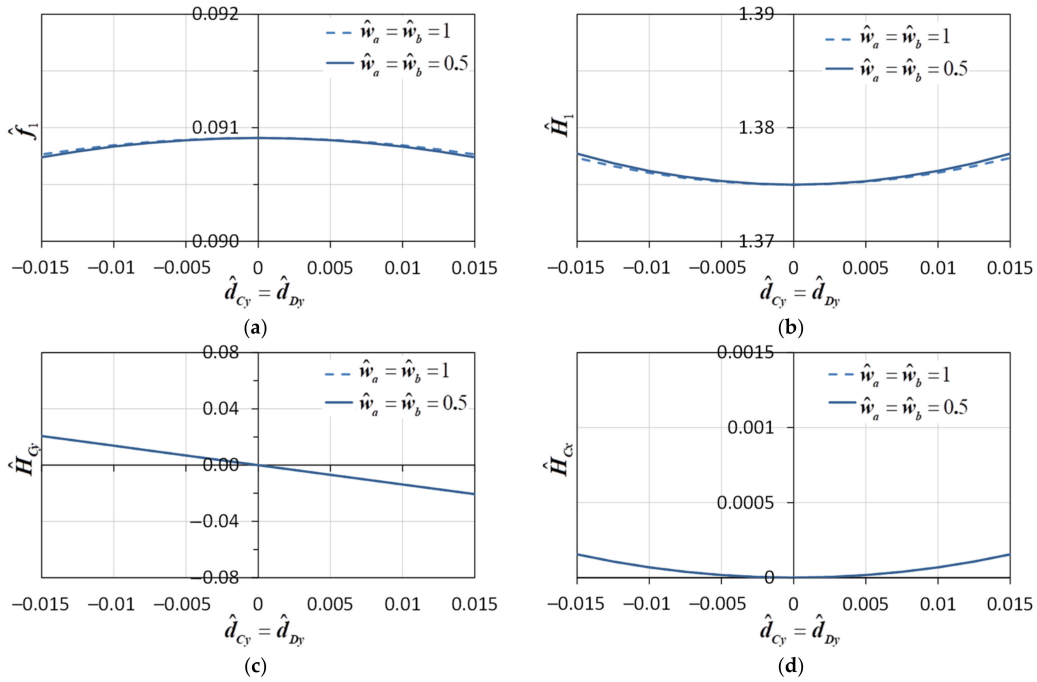

Figure 16. Variation in (**a**) $\hat{f}_1$, (**b**) $\hat{H}_1$, (**c**) $\hat{H}_{Cy}$, and (**d**) $\hat{H}_{Cx}$ due to $\hat{d}_{Cy} = \hat{d}_{Dy} \neq 0$.

With the same hypothesis as that of the previous case, the transversal bending moments at N and P will be equal to $3.6EI_z/L \cdot \hat{d}_{Dy}$ and $-3.6EI_z/L \cdot \hat{d}_{Dy}$, respectively. The transversal forced on the pylons will be $18EI_z/L^2 \cdot \hat{d}_{Dy}$ and $-18EI_z/L^2 \cdot \hat{d}_{Dy}$, at B and C, respectively. If the constraints are elastic or viscous-elastic, as usual to mitigate the effects of horizontal and seismic actions, the bending moments and the transversal forces will be lower that those given.

5.4. Rotation of a Tower

The rotation of a tower or, in general, the removal of the hypothesis that the abscissas of the corresponding anchorage points keep being equal, determines that the two cables have no longer the same geometry.

Consider the tower B subject to a vertical counterclockwise rotation β_B around its vertical axis (Figure 17). All the joints keep their coordinates, except for B and B′, whose displacements are

$$d_{Bx} = -d_{B'x} = B/2 \cdot \sin\beta_B \qquad d_{By} = -d_{B'y} = B/2 \cdot (1 - \cos\beta_B) \tag{21}$$

In the following numerical investigation, the value $\hat{B} = B/L = 1/60$ of the distance between the two parallel cables has been assumed. This value also is relative to long-span suspension bridges. The main and left-side spans change. In the hypothesis of small rotation, we can assume the following for cable A–B–C–D:

$$L_{a1} = \sqrt{(L_a + d_{Bx})^2 + d_{By}^2} \qquad L_1 = \sqrt{(L - d_{Bx})^2 + d_{By}^2} \tag{22}$$

In cable A′–B′–C′–D′, just the opposite happens: the side span reduces while the main span increases, the total span being the same. The effects on cable A–B–C–D in terms of sag ratio and horizontal force variations are shown in Figure 18. Changes in β_{a1} and β_1 are

very small, and so are the effects in terms of H_B and H_C, at least for technical values of β_B. For this reason, these have not been plotted.

In the reasonable range of rotation values for a tower, the effects on the deck are negligible.

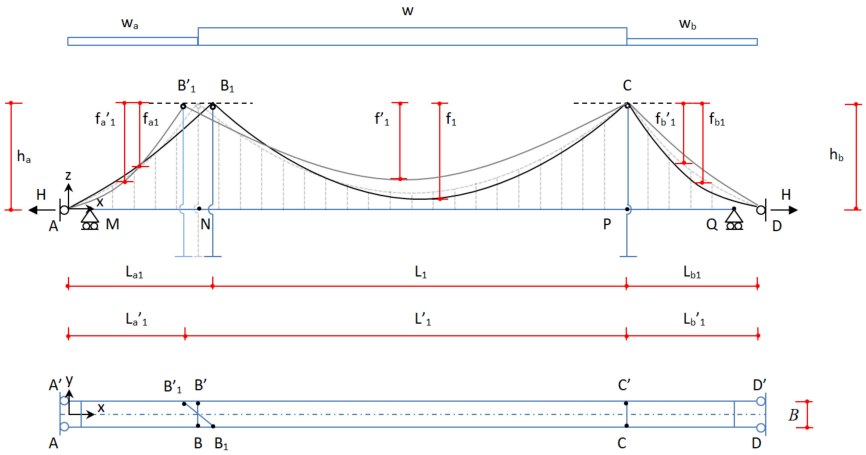

Figure 17. Effects of tower rotation β_B.

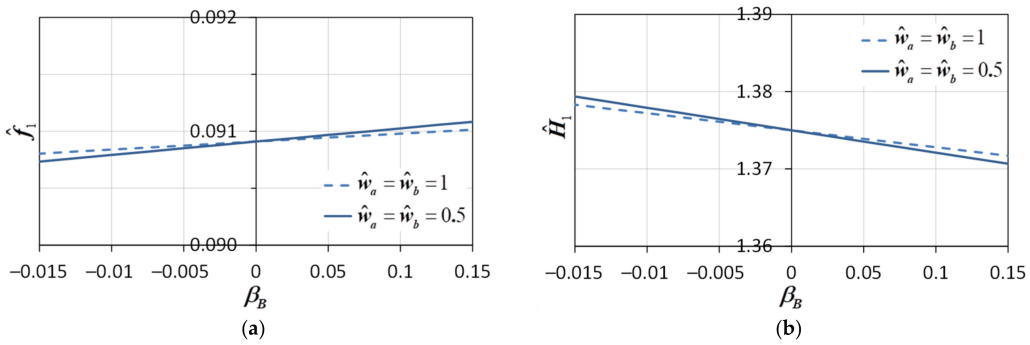

Figure 18. Variation in (**a**) $\hat{f}_1$ and (**b**) $\hat{H}_1$ due to $\beta_B \neq 0$.

6. A Simple Procedure for the Cable Check

As described in the previous paragraphs, any distortion causes a variation in the sag ratio of the main span, which translates into a variation in horizontal force and cable stress under dead loads. Two cases can occur:

- If the tension under the dead load increases, then the values of the travelling and other variable loads that the bridge can support will reduce.
- If the tension under dead load decreases, the cable deformability increases and the capacity of the bridge to support heavy travelling loads decreases.

In the new configuration, when the relative displacements have occurred, the value of the maximum stress under dead loads can be computed as follows:

$$\sigma_1 = \frac{H_1}{A}\sqrt{1+\left(4\hat{f}_1\right)^2} = \frac{\hat{L}_1}{\left(1-\hat{h}_1/2\hat{f}_1\right)}\frac{\sqrt{1/\hat{f}_1^2+16}}{\sqrt{1/\hat{f}^2+16}}\cdot\alpha f_d = \alpha_1 f_d \tag{23}$$

where

$$\alpha_1 = \frac{\hat{L}_1}{\left(1-\hat{h}_1/2\hat{f}_1\right)}\frac{\sqrt{1/\hat{f}_1^2+16}}{\sqrt{1/\hat{f}^2+16}}\cdot\alpha \leq 1 \tag{24}$$

is the parameter to check.

Consider the elementary cases already discussed before.

In Figure 19a, the factor α_1 is plotted versus the relative displacement $\hat{d}_{Dx}$. From the diagrams, one can see that for the assumed geometrical and mechanical characteristics, the

cable is within safety conditions as long as $\hat{d}_{Dx} < 0.0088$ or $\hat{d}_{Dx} < 0.0075$, for $\hat{w}_a = \hat{w}_b = 1$ and $\hat{w}_a = \hat{w}_b = 0.5$, respectively. Analogously, under relative displacements $\hat{d}_{Cx} = \hat{d}_{Dx}$, the cable is within safety conditions as long as $\hat{d}_{Dx} < 0.0075$ or $\hat{d}_{Dx} < 0.0065$, for $\hat{w}_a = \hat{w}_b = 1$ and $\hat{w}_a = \hat{w}_b = 0.5$, respectively (Figure 19b). In these two cases, negative values of the relative displacements determine very low changes in α_1, not significant for the stability of the bridge.

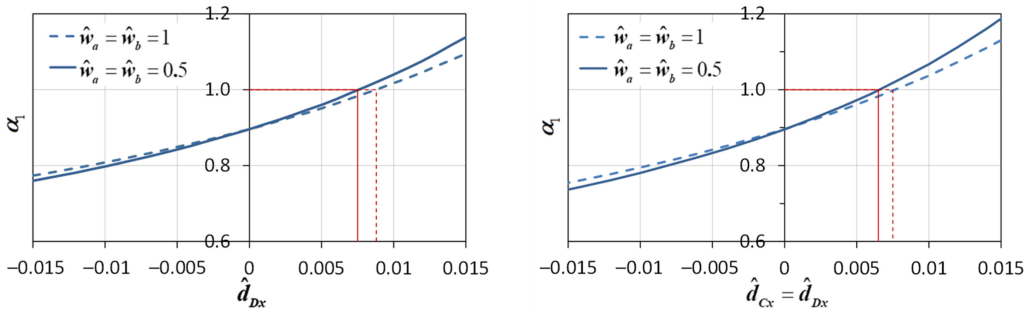

Figure 19. Variation in α_1 due to (**a**) $\hat{d}_{Dx} \neq 0$ and (**b**) to $\hat{d}_{Cx} = \hat{d}_{Dx} \neq 0$.

In Figure 20a, the values of α_1 are plotted versus the relative displacement $\hat{d}_{Dz}$. The cable is within safety conditions as long as $\hat{d}_{Dx} > -0.01$ or $\hat{d}_{Dx} > -0.009$, if $\hat{w}_a = \hat{w}_b = 1$ or $\hat{w}_a = \hat{w}_b = 0.5$, respectively. It is worth noting that an uplift of D alone has greater effects than that a simultaneous uplift of joints C and D of equal magnitude (Figure 20b). In this case, due to the symmetry, negative relative displacements have the same effects. Changes in cable tension due to transversal relative displacements are very low, as one can see from Figure 21a,b. The same is true for the rotation of a tower (Figure 22).

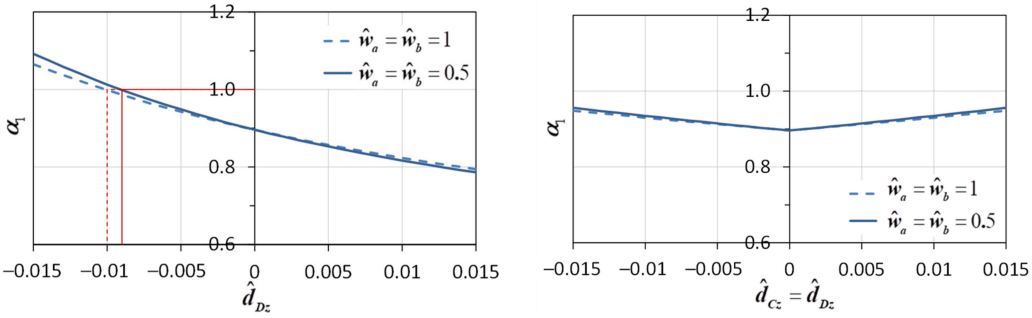

Figure 20. Variation in α_1 due to (**a**) $\hat{d}_{Cz} \neq 0$ and (**b**) to $\hat{d}_{Cz} = \hat{d}_{Dz} \neq 0$.

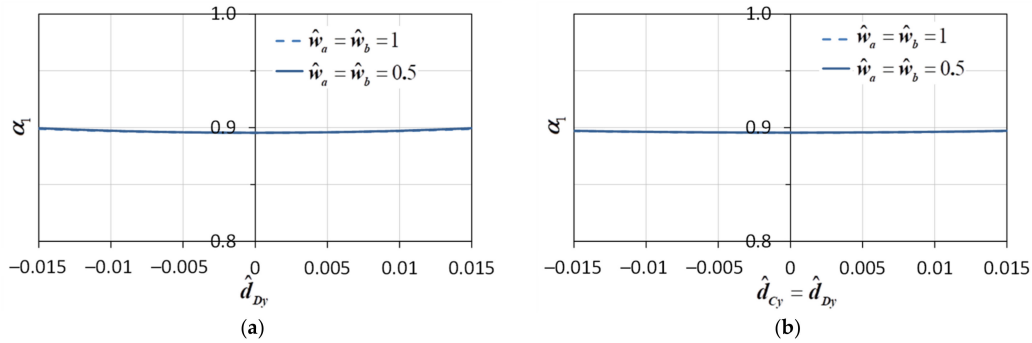

Figure 21. Variation in α_1 due to (**a**) $\hat{d}_{Cy} \neq 0$ and (**b**) to $\hat{d}_{Cy} = \hat{d}_{Dy} \neq 0$.

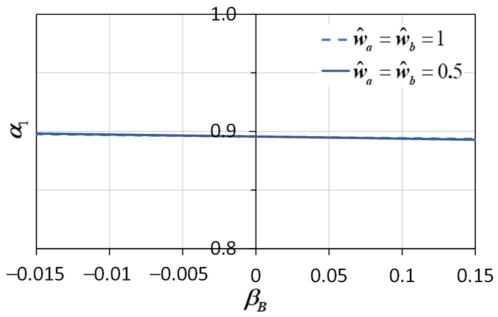

Figure 22. Variation in α_1 due to $\beta_B \neq 0$.

From the analysis of the various cases, it is apparent that the sag ratio of the main span varies linearly in the range of plausible relative displacements, which are certainly to be considered as very small displacements. This occurrence allows us to superimpose the effects in terms of sag variations and then calculate the final stress σ_1 in the new configuration.

The sag ratio in the main span due to n distortions can be evaluated as

$$\hat{f}_1 = \frac{f_1}{L_1} = \frac{f}{L_1} + \sum_i \frac{\Delta f_{1i}}{L_1} = \frac{\hat{f}}{\hat{L}_1} + \sum_i \Delta \hat{f}_{1i} \frac{\hat{L}_{1i}}{L_1} \tag{25}$$

where

$$\hat{L}_1 = 1 + \sum_i (\hat{L}_{1i} - 1) \tag{26}$$

As an example, consider the longitudinal displacement of C and D and the vertical displacement of D, which give the higher effects among the cases analyzed. For simplicity, suppose that these occur simultaneously with the same values. By superimposing the effects in terms of the variation in the sag ratio, the diagrams of Figure 23 are obtained. From these, it can be seen that, in this particular case, the cable is within safety conditions up to displacements $\hat{d}_{Cx} = \hat{d}_{Dx} = \hat{d}_{Dz}$ equal to 0.0045 and 0.0038 for $\hat{w}_a = \hat{w}_b = 1$ and $\hat{w}_a = \hat{w}_b = 0.5$, respectively. If the trend of these displacements is known, a suitable time for an intervention can be estimated, if needed, over the lifetime of the bridge.

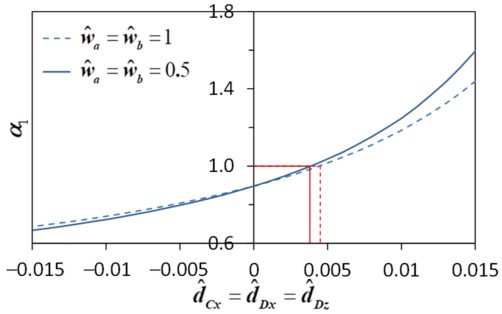

Figure 23. Variation in α_1 due to $\hat{d}_{Cx} = \hat{d}_{Dx} = \hat{d}_{Dz}$.

7. Discussion and Conclusions

The effects of relative displacements between the ground anchors of a suspension bridge strongly influence its structural design. The displacements can arise both from slow tectonic shifts and/or seismic events and vary by up to several metres. While the seismic effects on ordinary bridges crossing fault rupture zones have been studied by several authors, very few works have faced the effects of tectonic shifts in suspension bridges.

Nowadays, sophisticated finite element codes are available, which allow us to model the actual behaviour of suspension bridges, accounting for the nonlinearities and the various features of their complex behaviour.

In this context, it is important to have a simple model, such as that proposed here, which can be easily implemented via computer software. The model is based on well-

known and consolidated equilibrium and compatibility relationships, and is very useful for a fast preliminary analysis, providing the ability to point out risk situations that deserve to be analyzed in depth. It refers to the behaviour of the main cables only, while the effects on towers and deck are assessed as a consequence of the previous ones.

A numerical investigation, carried out with reference to a model having the typical geometrical and mechanical characteristics of very long span suspension bridges, pointed out that realistic relative displacements between its anchors to the ground do not significantly affect the stresses in the structure and the effects become negligible as the span increases. The results are given in simple diagrams that can be easily used for a preliminary check. The main results, to be consider in the design, can be summarized as follows:

- The variations in the sag ratio and the horizontal force in the cables are very low and therefore not dangerous if longitudinal relative displacements are lower than $0.0065 \cdot L$ or vertical relative displacements are lower than $0.009 \cdot L$, while the transversal relative displacements and the rotation of a tower have no significant effects.
- In the case of multiple distortions, using the superposition of the effects for the sag variations and then calculating the stress in the cables, the limits given above may be reduced. Considering a superimposition of the longitudinal displacement of C and D with a vertical displacement of D, a threshold value of $0.0038 \cdot L$ has been obtained. For higher values of the displacements, the variations could become very high, both in terms of the sag ratio and horizontal force. Nevertheless, these values of displacements would be unrealistic.
- Even lower limit values should be considered to take into account the possible seismic effects, which would be added to the slow tectonic ones.
- Transversal displacements generate horizontal forces at the top of the pylons in the longitudinal direction. Even though the values of these forces are quite low, this occurrence should be accounted for carefully.
- The effects on the deck, which has been supposed to be simply supported in the vertical direction at its ends A and D and rigidly constrained in the transversal direction at the same sections and at the pylons, have been evaluated in a qualitative way. An accurate assessment should consider the geometric nonlinearities and therefore the setup of a suitable mathematical model.

One of the issues under discussion is what to plan for when designing new bridges or when retrofitting existing ones to avoid or mitigate these effects.

If needed, the internal forces caused by these displacements can be significantly reduced by inserting spherical hinges at the sections between the main and the side spans, as already proposed in notable cases, so the relative rotations with reference to both the vertical and the horizontal axes could be allowed. The effects in the case of a railway bridge must be accurately analyzed.

In any case, the control of the effects of these distortions on structural details, such as joints and constraints, is of fundamental importance for suspension bridges. The use of satellite technologies allows us to obtain frequent, accurate, and substantially accessible information. Radar data are particularly interesting as they allow the monitoring of the surface movements of the territory and so also the identification and prevention of landslide phenomena and ground instability.

A suitable monitoring strategy allows maintenance interventions to be performed on sensitive details during the life of a bridge, which could already be taken into account at the design stage. Expansion and seismic joints, as well as support devices and constraints, can be replaced, including control devices, thus extending the lifespan of a suspension bridge.

Funding: This research received no external funding.

Data Availability Statement: Data are contained within the article.

Conflicts of Interest: The authors declare no conflict of interest.

References

1. Pugsley, A. *The Theory of Suspension Bridges*, 2nd ed.; Arnold LTD: London, UK, 1968.
2. Buonopane, S.G.; Billington, D.P. Theory and History of Suspension Bridge Design from 1923 to 1940. *J. Struct. Eng.* **1993**, *119*, 954–977. [CrossRef]
3. Rockland, M.A. *The George Washington Bridge: Poetry in Steel*; Rutgers University Press: New York, NY, USA, 2020. [CrossRef]
4. Cassady, S. *Spanning the Gate*; Square Books: Santa Rosa, CA, USA, 1986.
5. Brancaleoni, F.; Diana, G. The aerodynamic design of the Messina Straits Bridge. *J. Wind. Eng. Ind. Aerodyn.* **1993**, *48*, 395–409. [CrossRef]
6. Diana, G.; Falco, M.; Cheli, F.; Cigada, A. The Aeroelastic Study of the Messina Straits Bridge. *Nat. Hazards* **2003**, *30*, 79–106. [CrossRef]
7. Lin, T.Y.; Chow, P. Gibraltar Strait Crossing—A Challenge to Bridge and Structural Engineers. *Struct. Eng. Int.* **1991**, *1*, 53–58. [CrossRef]
8. Clemente, P.; Bongiovanni, G.; Buffarini, G.; Saitta, F. Structural health status assessment of a cable-stayed bridge by means of experimental vibration analysis. *J. Civ. Struct. Health Monit.* **2019**, *9*, 655–669. [CrossRef]
9. Kurata, M.; Kim, J.; Lynch, J.P.; Van der Linden, G.W.; Sedarat, H.; Thometz, E.; Hipley, P.; Sheng, L.-H. Internet-Enabled Wireless Structural Monitoring Systems: Development and Permanent Deployment at the New Carquinez Suspension Bridge. *J. Struct. Eng.* **2013**, *139*, 1688–1702. [CrossRef]
10. Koo, K.Y.; Brownjohn, J.M.W.; List, D.I.; Cole, R. Structural health monitoring of the Tamar suspension bridge. *Struct. Control. Health Monit.* **2013**, *20*, 609–625. [CrossRef]
11. Comanducci, G.; Ubertini, F.; Materazzi, A.L. Structural health monitoring of suspension bridges with features affected by changing wind speed. *J. Wind. Eng. Ind. Aerodyn.* **2015**, *141*, 12–26. [CrossRef]
12. Ni, Y.-Q.; Xia, Y.-X. Strain-Based Condition Assessment of a Suspension Bridge Instrumented with Structural Health Monitoring System. *Int. J. Struct. Stab. Dyn.* **2016**, *16*, 1640027. [CrossRef]
13. William, G.W.; Shoukry, S.N.; Riad, M.Y. Structural health monitoring of a historical suspension bridge. In *Asset Management of Bridges, Proceedings of the 9th New York City Bridge Conference, New York, NY, USA, 21–22 August 2017*; CRC Press: Boca Raton, FL, USA, 2017; pp. 213–226.
14. Sheng, Y.; Jinping, O. Structural health monitoring and model updating of Aizhai Suspension Bridge. *J. Aerosp. Eng.* **2017**, *30*, B4016009. [CrossRef]
15. Xueshan, L.; Xiaohu, C.; Jianting, Z.; Xiaogang, L. Research on long-term health monitoring and operation evaluation system for long-span self-anchored suspension bridge. In *Bridge Maintenance, Safety, Management, Life-Cycle Sustainability and Innovations, Proceedings of the 10th Int. Conf. IABMAS 2020, Sapporo, Japan, 11–15 April 2021*; CRC Press: Boca Raton, FL, USA, 2021; pp. 151–157. [CrossRef]
16. Clemente, P. Monitoring and evaluation of bridges. Lessons from the Polcevera Viaduct collapse in Italy. *J. Civ. Struct. Health Monit.* **2020**, *10*, 177–182. [CrossRef]
17. Ormando, C.; Lucaferri, V.; Giocoli, A.; Clemente, P.; Buffarini, G.; Tofani, A. Index of Attention for a simplified condition assessment and classification of bridges. *Infrastructures* **2024**, *9*, 125. [CrossRef]
18. Buffarini, G.; Clemente, P.; Giovinazzi, S.; Ormando, C.; Scafati, F. Structural assessment of the pedestrian bridge accessing Civita di Bagnoregio, Italy. *J. Civ. Struct. Health Monit.* **2023**, *13*, 1499–1516. [CrossRef]
19. Antonioli, F.; Sylos Labini, S.; Ferranti, L. Il Ponte sullo Stretto: Problematiche geologiche. *Energ. Ambiente E Innov.* **2002**, *1*, 63–67.
20. Sulli, A.; Lo Presti, V.; Morticelli, M.G.; Antonioli, F. Vertical movements in NE Sicily and its offshore: Outcome of tectonic uplift during the last 125 ky. *Quat. Int.* **2013**, *288*, 168–182. [CrossRef]
21. Lo Presti, V.; Antonioli, F.; Casalbore, D.; Chiocci, F.L.; Lanza, S.; Sulli, A.; Randazzo, G. Geohazard assessment of the north-eastern Sicily continental margin (SW Mediterranean): Coastal erosion, sea-level rise and retrogressive canyon head dynamics. *Mar. Geophys. Res.* **2022**, *43*, 2. [CrossRef]
22. Abdel-Ghaffar, A.M.; Scanlan, R.H. Ambient Vibration Studies of Golden Gate Bridge: I. Suspended Structure. *J. Eng. Mech.* **1985**, *111*, 463–482. [CrossRef]
23. Doglioni, C.; Ligi, M.; Scrocca, D.; Bigi, S.; Bortoluzzi, G.; Carminati, E.; Cuffaro, M.; D'Oriano, F.; Forleo, V.; Muccini, F.; et al. The tectonic puzzle of the Messina area (Southern Italy): Insights from new seismic reflection data. *Sci. Rep.* **2012**, *2*, 970. [CrossRef]
24. Barreca, G.; Gross, F.; Scarfì, L.; Aloisi, M.; Monaco, C.; Krastel, S. The Strait of Messina: Seismotectonics and the source of the 1908 earthquake. *Earth-Sci. Rev.* **2021**, *218*, 103685. [CrossRef]
25. Yamagata, M.; Yasuda, M.; Nitta, A.; Yamamoto, S. Effects on the Akashi Kaikyo Bridge. *Soils Found.* **1996**, *36*, 179–187. [CrossRef]
26. Yang, S.; Mavroeidis, G.P. Bridges crossing fault rupture zones: A review. *Soil Dyn. Earthq. Eng.* **2018**, *113*, 545–571. [CrossRef]
27. Hongyu, J.; Yang, J.; Zheng, S.; Canhui, Z.; Xiuli, D. A review on aseismic bridges crossing fault rupture regions. *J. Southwest Jiaotong Univ.* **2020**, *2*, 20–36.
28. Lin, Y.; Zong, Z.; Lin, J.; Li, Y.; Chen, Y. Across-fault ground motions and their effects on some bridges in the 1999 Chi-Chi earthquake. *Adv. Bridge Eng.* **2021**, *2*, 8. [CrossRef]
29. Goel, R.K.; Chopra, A.K. Nonlinear analysis of ordinary bridges crossing fault-rupture zones. *J. Bridge Eng.* **2009**, *14*, 216–224. [CrossRef]

30. Jia, H.; Jia, K.; Sun, C.; Li, Y.; Zhang, C.; Zheng, S. Preliminary numerical study on seismic response of ordinary long-span suspension bridges crossing active faults. *Adv. Bridge Eng.* **2021**, *2*, 16. [CrossRef]
31. Clemente, P.; Nicolosi, G.; Raithel, A. Preliminary design of very long-span suspension bridges. *Eng. Struct.* **2000**, *22*, 1699–1706. [CrossRef]
32. Kawada, T. *History of the Modern Suspension Bridge Solving the Dilemma Between Economy and Stiffness*; ASCE Press: Reston, VA, USA, 2010; 262p.
33. Wang, H.; Chen, Q.; Agrawal, A.K.; El-Tawil, S.; Bhattacharya, B.; Wong, W. Performance of a Long-Span Suspension Bridge Subjected to Sudden Single Suspender Loss. *J. Bridge Eng.* **2023**, *28*, 05023006. [CrossRef]